Biosensors and Bioelectronics 141 (2019) 111431

Contents lists available at ScienceDirect

Biosensors and Bioelectronics

journal homepage: www.elsevier.com/locate/bios

Amperometric sarcosine biosensor with strong anti-interference capabilities based on mesoporous organic-inorganic hybrid materials

Qia Wang[a,1], Yuting Zhao[a,1], Qingui Yang[a], Dan Du[b], Haipeng Yang[a,**], Yuehe Lin[b,*]

[a] College of Materials Science and Engineering, Shenzhen Key Laboratory of Polymer Science and Technology, Shenzhen University, Shenzhen, 518060, PR China
[b] School of Mechanical and Material Engineering, Washington State University, Pullman, WA, 99164, United States

ARTICLE INFO

Keywords:
Amperometric biosensor
Anti-interference
Prostate cancer screening
Sarcosine
Surface potential

ABSTRACT

Amperometric enzyme biosensors are some of the simplest and cheapest types of medical devices used in the rapid detection of biomarkers that have been developed in the past fifty years. When the concentrations of biomarkers are at micromoles per liter, such as for sarcosine, which was recently discovered as a biomarker for prostate cancer, the response signal of the interferences is huge, and the biosensor is hard to satisfy the requirements of practical applications. In this manuscript, we describe a strategy for synthesizing a surface electronegative organic-inorganic hybrid mesoporous material, which could reduce the interference signal much better than Nafion and Chitosan. We verify that the surface potential of the carrier nanomaterial plays an important role in excluding anionic interferences. We also prepare a sensitive (16.35 μA mM^{-1}), low LOD (0.13 μM) and wide linear range (1–70 μM) amperometric sarcosine biosensor with excellent anti-interference properties. This mesoporous material provides a bio-composite platform for the development of simple amperometric biosensors for detecting micromoles per liter of analytes in serum or urine.

1. Introduction

Prostate cancer (PCa) is an epithelial malignancy that seriously influences the health of men (Damber and Aus, 2008; Hassanipour-Azgomi et al., 2016; Tombach et al., 2001). No obvious symptoms for patients appear in incipient stages. However, it has developed into its advanced stage when some symptoms such as hematuria were found, so the early detection of PCa is of great significance for reducing mortality and improving the quality of life for patients (Penson et al., 2003). At present, the prostate specific antigen (PSA) test is the most widely used test in clinical diagnosis (Lilja et al., 2008). However, some studies have demonstrated that the expression of PSA is influenced by multitudinous pathological and physiological factors, resulting in fallacious detection (Logozzi et al., 2017; Sun et al., 2011; Thompson et al., 2004). Therefore, more reliable and specific biomarkers are desired for the detection of PCa. In 2009, Sreekumar and co-workers found that sarcosine in serum or urine is a biomarker for PCa (Sreekumar et al., 2009). However, the very low concentration of sarcosine makes its detection methods sophisticated, high cost or needs skilled person, which are not suitable for clinical popularization (Jiang et al., 2010; Meyer et al., 2011). Amperometric enzyme biosensors are a very simple and low-cost type of rapid detection device. However, due to the coexistence of interfering substances in serum or urine, an amperometric sarcosine biosensor based on sarcosine oxidase (SOx) cannot satisfy the demands of practical application (Yang et al., 2018). The principle for electrochemical detection of sarcosine using SOx is as follows (Rebelo et al., 2014; Zhou et al., 2012):

$$\text{Sarcosine} + O_2 + H_20 \xrightarrow{SOx} \text{Glycine} + H_2O_2$$

By detecting hydrogen peroxide (H_2O_2), one of the reaction products, the concentration of sarcosine in urine or serum can be detected indirectly. For example, Kumar and coworkers immobilized SOx onto a gold electrode to fabricate an outstanding amperometric sarcosine biosensor (Kumar et al., 2018); Rebelo's group prepared a carbon screen printed electrode modified with sarcosine oxidase on the electrode surface that was used to successfully analyze sarcosine in urine samples (Rebelo et al., 2014); Vinay Narwal and coworkers fabricated an excellent sarcosine biosensor modified with chitosan/CuNPs/c-MWCNT (Narwal et al., 2018). As we know, Nafion and Chitosan are the two commonly used anti-interfering film on biosensors. Most of the previously reported sarcosine biosensors usually use Nafion or chitosan to

* Corresponding author.
** Corresponding author.
E-mail addresses: yanghp@szu.edu.cn (H. Yang), yuehe.lin@wsu.edu (Y. Lin).
[1] These authors contributed equally to this work.

https://doi.org/10.1016/j.bios.2019.111431
Received 6 May 2019; Received in revised form 5 June 2019; Accepted 8 June 2019
Available online 13 June 2019
0956-5663/

reduce interfering signal. One of a study of Kumar et al. prepared SOx nanoparticles to improve the analytic performance of sarcosine biosensor (Kumar et al., 2018). This is very valuable. However, this study does not discuss the reasons of its good anti-interference property, especially with such a high voltage of 1 V vs. Ag/AgCl. In such a high voltage, Au electrode usually has remarkable interference signal and is hard to be used to detect sarcosine (Rebelo et al., 2014). In one word, the anti-interference performance of sarcosine biosensors still needs further studies.

Platinum (Pt), which is used as a catalyst, exhibits excellent catalytic activity and reusability with respect to H_2O_2 (Bai et al., 2016; Guo et al., 2010; Serra-Maia et al., 2018). However, due to the existence of Pt nanoparticles, electroactive interfering substances are extremely prone to form interference signals when detecting low concentration levels of substances, resulting in distorted current signal. On the other hand, Pt nanoparticles are easily agglomerated due to their high surface energy and surface activity, which significantly reduces the amount of catalytic active sites (Chung et al., 2015; Narayanan and El-Sayed, 2004; Shi et al., 2015). Therefore, how to eliminate the influence of electroactive interfering substances and prevent the agglomeration of Pt nanoparticles is of great significance for amperometric enzyme biosensors. Covering anti-interference layer is a commonly used method to exclude interfering substances. However, it is not only inconvenient, but it may also influence the transfer of electrons. Therefore, the anti-interference layer cannot completely satisfy the demand of practical application. Compared with the anti-interference layer, there is a more effective path towards enhancing the anti-interference performance via adjusting the charges on the surfaces of materials (Song et al., 2018). Organic-inorganic hybrid mesoporous materials have several advantages as an ideal base material (Benzigar et al., 2018; Hoffmann et al., 2006; Li and Shi, 2014; Walcarius, 2013; Wang et al., 2018; Wei et al., 2017). For example, their three-dimensional porous structure can greatly reduce the agglomeration of particles, improving catalytic efficiency and utilization. Mesoporous structures with good biocompatibility also provide sufficient space for the chemical reactions of electroactive substances. Compared with traditional porous materials with pure inorganic frameworks, the organic-inorganic hybrid porous material is endowed with more possibilities. This is because its skeleton is comprised of different types of organic groups and inorganic species, which allows for the organic functional group skeleton to be flexibly controlled, achieving the desired surface charge modulation.

Herein, we describe a simple strategy for synthesizing surface electronegative platinum-supported organic-inorganic hybrid mesoporous molybdenum phosphonate (Pt/OIHMMP) and preparing an excellent anti-interference sarcosine biosensor (Scheme 1). The agglomeration of Pt particles was greatly reduced due to the mesoporous structure. Thus, the Pt particles reduced by $PtCl_6^{2-}$ via the immersion reduction method were uniformly dispersed on the surface of OIHMMP, which endows Pt/OIHMMP with excellent electrocatalytic activity towards H_2O_2. Additionally, glutaraldehyde and bovine serum albumin were used as co-cross linking agents to immobilize SOx, permitting the SOx to be uniformly distributed on the Pt/OIHMMP, which maintained its bioactivity. When sarcosine arrives at the active sites of SOx, it is oxidized to produce glycine, formaldehyde and H_2O_2. Subsequently, the H_2O_2 transfers to the Pt/OIHMMP and is oxidized to generate current (Cui et al., 2014). The current is proportional to the concentration of sarcosine, achieving a sensitive sarcosine biosensor. Thus, the Pt/OIHMMP-based sarcosine biosensor has great potential application prospects in the screening and diagnosis of PCa. In addition, it has the potential to be extended to other types of oxidase reactions.

2. Experimental

2.1. Materials

Ethylenediamine tetramethylene phosphonic acid (Fig. S1, supporting information), chloroplatinic acid hexahydrate ($H_2PtCl_6 \cdot 6H_2O$), hexadecyl trimethyl ammonium bromide (CTAB), sodium hydroxide (NaOH) and ammonium molybdate were purchased from Macklin Biochemical Co., Ltd. (Shanghai, China). Anhydrous ethanol, glutaraldehyde, sodium borohydride and hydrochloric acid (HCl) were purchased from Jinhuada Chemical Reagent Co., Ltd. (China, Guangzhou). Sarcosine oxidase (37 unit mg^{-1}) and bovine serum albumin were procured from J&K Scientific Company. The hydrogen peroxide solution with a mass fraction of 30% was obtained from Shanghai Aladdin Bio-Chem Technology Co., Ltd. Serum samples were purchased from Huayang Zhenglong (Chengdu, China). Deionized water was used to prepare the solution and clean the electrode. Sarcosine was produced by Acros Organics Company. The chemicals used in our work were of analytical reagent grade.

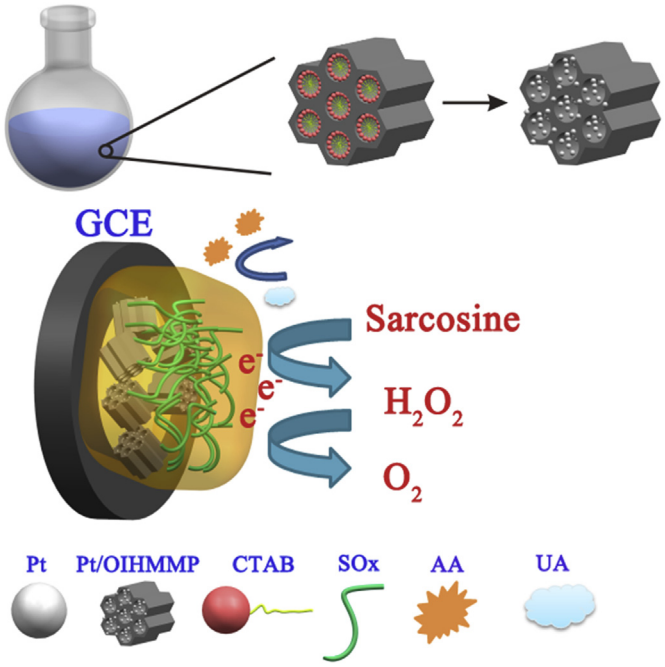

Scheme 1. The preparation of SOx/Pt/OIHMMP/GCE and its application for sarcosine detection.

2.2. Characterizations

Scanning electron microscope (SEM) images were obtained using an SU-70 (5 kV, Hitachi, Japan). Energy dispersive spectrometer (EDS) data were characterized using an X-Maxn (15 kV, Oxford instrument, Britain). X-ray diffraction (XRD) patterns were collected using a Bruker D8 Advance (Germany, 3–85°, 5° min^{-1}). Nitrogen adsorption desorption data was collected with an instrument (Micromeritics ASAP, 2020 HD88, N_2, 77 K). Transmission electron microscope (TEM) images were taken using a Tecnai G2 F30 (Thermo Fisher Scientific, 300 kV). Infrared spectrum data were recorded using a Nicolet 6700 Fourier transform infrared spectrometer. Electrochemical measurements were performed using a CHI 660C workstation (Chen Hua Instrument Co. Ltd, Shanghai). Zeta potential data was obtained using a Zetasizer Nano ZS90 (Malvern, Britain).

2.3. Synthesis of Pt/OIHMMP

2 g of CTAB, 0.436 g of EDTMPA and 0.32 g of NaOH were dissolved in 20 g of deionized water. The mixed solution was heated in a water bath (30 min, 45 °C) to obtain solution 1.9.408 g of ammonium molybdate were dissolved in 5 g of deionized water (solution 2). Solution 2 was added into solution 1 and heated in a water bath (2 h, 45 °C). The

mixture was transferred into an autoclave for aging (24 h, 120 °C), rinsing (deionized water, three times) and drying (60 °C). The obtained powder was mixed with 15 mL HCl and 15 mL anhydrous ethanol and then heated in a water bath (6 h, 60 °C). Then, the pH value of the solution was adjusted to neutrality, and it was dried at 60 °C to obtain OIHMMP. Pt/OIHMMP was prepared by the following method: 3 g of OIHMMP and 3 mL of a solution of $H_2PtCl_6 \cdot 6H_2O$ (0.019 M) in ethanol were mixed for 24 h. Then, a solution of sodium borohydride (0.01 M) in ethanol was slowly dropped into the solution with stirring (120 min), followed by drying. The Pt/OIHMMP was obtained after calcining under a N_2 atmosphere (400 °C, 5 h).

2.4. Preparation of Pt/OIHMMP/GCE and SOx/Pt/OIHMMP/GCE

Alumina powder (0.3 and 1 μm) was used to polish the glassy carbon electrode (GCE, 3 mm in diameter), rinsing with deionized water and ethanol. A black suspension was obtained after mixing Pt/OIHMMP (10 mg) and deionized water (1 mL) and ultrasonication for 30 min. The Pt/OIHMMP/GCE was prepared by covering 10 μL of Pt/OIHMMP suspension on the GCE surface, using glutaraldehyde (0.1 M) as a co-cross linking agent and drying at room temperature (approximately 25 °C). Subsequently, 5 μL of 4 unit μL^{-1} (involving 7% bovine serum albumin) of SOx was immobilized on Pt/OIHMMP/GCE by using glutaraldehyde, marking it as SOx/Pt/OIHMMP/GCE, and then it was dried at room temperature (approximately 25 °C). The modified electrodes were immersed in PBS (0.1 M, pH = 7) and stored at 4 °C.

3. Results and discussion

3.1. Characterization of Pt/OIHMMP

The morphology of Pt/OIHMMP observed by SEM (Fig. 1a) is a typical three-dimensional porous morphology, which may be attributed to the organic skeleton. Through elemental mapping (Fig. 1b), the main elemental distribution (Mo, Pt, P and C) of Pt/OIHMMP was characterized, and it is clear that the Pt particles are uniformly dispersed on the surface of the OIHMMP, indicating the increases in the amount of catalytic active sites, which gives the Pt/OIHMMP excellent electrocatalytic activity toward H_2O_2. The EDS spectrum of Pt/OIHMMP is shown in Fig. S2. TEM images of Pt/OIHMMP (Fig. 1c and d) indicate a porous structure. The inset of Fig. 1d displays a high-resolution TEM image, depicting the typical spacing of 0.237 nm for the (111) lattice plane of face-centered cubic Pt, corresponding to the XRD peak at 40.02°. The XRD pattern of OIHMMP and Pt/OIHMMP is displayed in Fig. S3. Compared with the OIHMMP, Pt/OIHMMP has several peaks at 46.72°, 67.22° and 81.73°, corresponding to the other three characteristic diffraction peaks of Pt (JCPDS 65–2868), which are identified as the (200), (220) and (311) lattice plane, respectively. This also demonstrates that the Pt particles were successfully reduced.

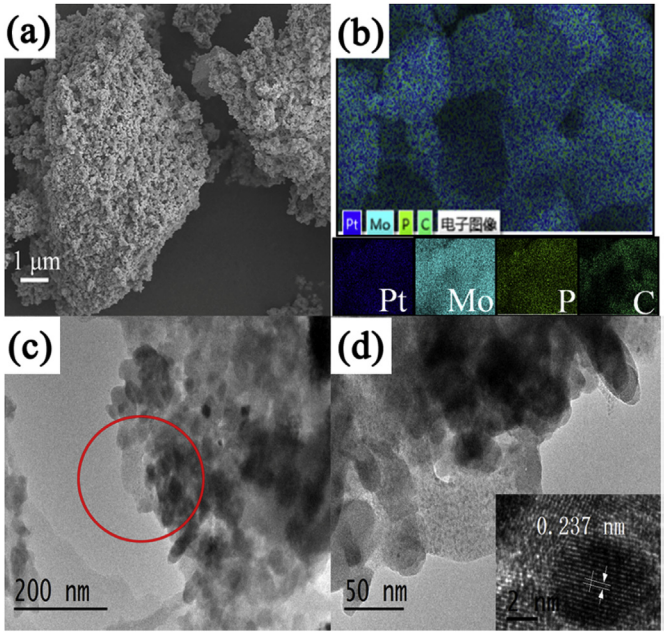

Fig. 1. (a) SEM image, (b) Element mapping image and main elemental distribution; (c) TEM image of Pt/OIHMMP; (d) Partially magnified area of (c). The inset shows the high-resolution TEM image.

As a porous material, the specific surface area (369 $m^2 g^{-1}$) and pore volume (0.634 $cm^3 g^{-1}$) of Pt/OIHMMP used here were characterized by nitrogen sorption (Fig. 2a). The inset of Fig. 2a exhibits the corresponding pore differential distribution curve, displaying a wide distribution in the range of 4–28 nm. On the basis of the classification of nitrogen sorption by IUPAC (Sing et al., 1985), the sorption isotherm seen here should be classified as Class IV H3, showing a mesoporous structure with typically connective pores. There is a large and non-parallel hysteresis loop in the high relative pressure zone, which indicates that the porous structure was formed by mutual accumulation and the presence of large secondary pores. The Fourier infrared spectroscopy pattern of Pt/OIHMMP and organic acid EDTMPA (Fig. 2b) displays a broad band at 632 cm^{-1}, which can be attributed to a P–O–Mo stretching vibration and a weak band at 972 cm^{-1} that is due to P–OH. Three neighboring bands at 1321, 1364 and 1428 cm^{-1} should be identified as the stretching vibrations of C–N, P═O and P–C, respectively. The sharp band and broad band at 1634 and 3410 cm^{-1}, respectively correspond to the surface adsorbed water and hydroxyl groups (Zhang et al., 2008). Additionally, weak bands at 2849 and 2926 cm^{-1} can be attributed to the stretching vibrations of the C–H in methylene groups of the organic coupling components. According to the above results, Pt/OIHMMP was successfully synthesized and the skeleton of EDTMPA was not destroyed after calcinations.

3.2. The electrochemical performance of Pt/OIHMMP/GCE for reaction product (H_2O_2)

The electrochemical properties of Pt/OIHMMP/GCE to H_2O_2 were firstly studied. The cyclic voltammetry (CV) curves (Fig. 3a) of Pt/OIHMMP/GCE depict a phenomenon in which the potential of the anode and cathode peaks remains stable, while the peak current gradually increases with increasing scanning rate, indicating that Pt/OIHMMP/GCE has excellent electrochemical reaction capabilities and electron transfer kinetics. A quality linear relationship between the anodic and cathodic peaks' current and square root of scan rate (the inset of Fig. 3a) indicates that the kinetic process of Pt/OIHMMP/GCE is diffusion-controlled (Yang et al., 2014). As the H_2O_2 concentration increased from 0 mM to 10 mM (Fig. 3b), the current of the anodic peak is gradually increased. A favorable linear relationship (the inset of Fig. 3b) between the H_2O_2 concentration and peak current demonstrates that Pt/OIHMMP has good electrocatalytic activity for the oxidation of H_2O_2. A successive amperometric curve (Fig. 3c) indicates that Pt/OIHMMP/GCE has a fast response to different concentrations of H_2O_2 and quickly reaches a stable current. Fig. 3d depicts the corresponding linear relationship between the current and H_2O_2 level. It was divided into two stages: low range (1–2110 μM) and high range (2110–11110 μM). The linear regression equation and sensitivity in the range 1–2110 μM are $I(\mu A) = 0.01122C(\mu M) + 1.0825 (R^2 = 0.993)$ and 11.22 μA mM^{-1}, respectively. Compared with other platinum-supported H_2O_2 sensitive mesoporous materials (Table S1), the limit of detection (LOD) of Pt/OIHMMP (0.08 μM, S/N = 3) is lower. The enhanced electrocatalytic performance of Pt/OIHMMP/GCE may be attributed to the following aspects. First, Pt/OIHMMP has a large specific surface area, providing sufficient space for the reactions of electro-active substances. Second, the reduced Pt particles are uniformly

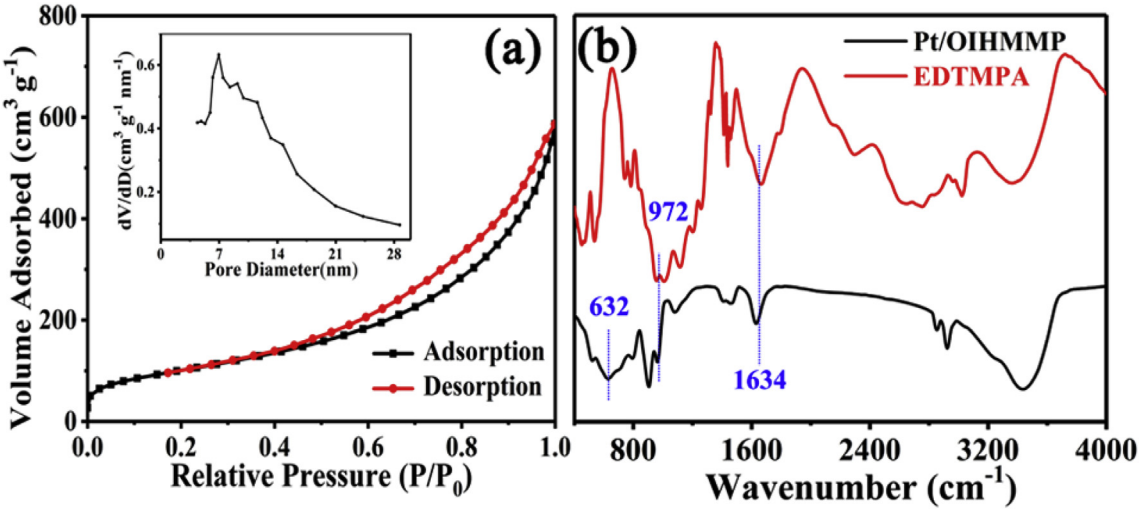

Fig. 2. (a) Nitrogen adsorption-desorption isotherm of Pt/OIHMMP. Inset displays the corresponding porous differential distribution curve; (b) Fourier infrared spectroscopy pattern of EDTMPA and Pt/OIHMMP.

dispersed on the surface of OIHMMP, increasing the large number of catalytic active sites. Finally, according to electrostatic theory, transitional elements are often prone to chemical reactions involving redox chemistry, free radical chemistry, photochemical reactions, and atomic extraction reactions (Huang et al., 2015; Kalantar-zadeh et al., 2015). Therefore, the electrocatalytic performance of Pt/OIHMMP/GCE regarding the oxidation of H_2O_2 is enhanced, indicating that Pt/OIHMMP is a positively sensitive material for H_2O_2. This is expected to be used as the base material for enzyme based biosensors.

Interference tests (Fig. S4a) and columnar error analysis (Fig. S4b) reveals that there is no interference in citric acid (CA), maltose and fructose in H_2O_2 detection. However, a very small response current was observed after injecting ascorbic acid (AA) and uric acid (UA), the main interfering substances in serum, suggesting that Pt/OIHMMP/GCE has

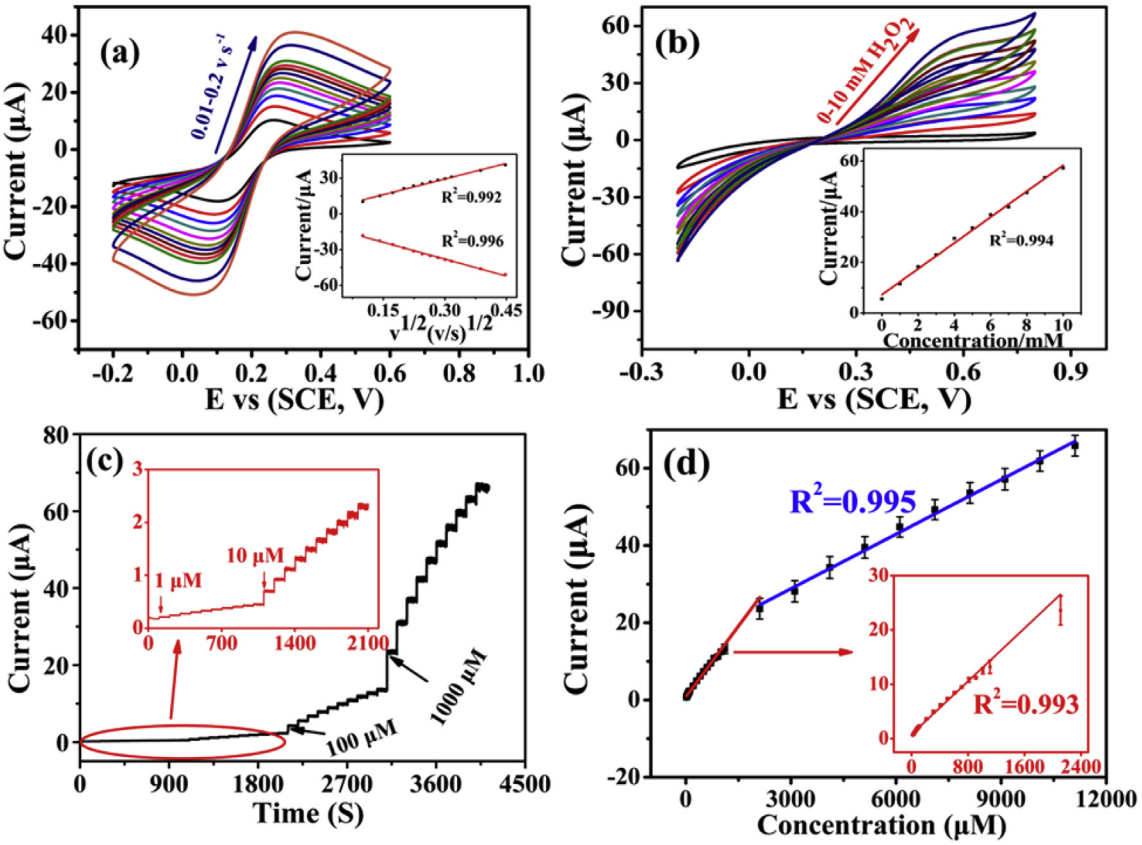

Fig. 3. CVs of Pt/OIHMMP/GCE, (a) in potassium ferricyanide solution (5 mM) with different scan rates (0.01, 0.02, 0.03, 0.04, 0.05, 0.06, 0.07, 0.08, 0.09, 0.1, 0.15 and 0.2 V s^{-1}). The illustration displays the relationship between the square root of the scan rate and peak current; (b) in the absence and presence of H_2O_2 (1, 2, 3, 4, 5, 6, 7, 8, 9, 10 mM) in PBS (0.1 M) with a scan rate of 50 mV s^{-1}. The illustration displays the relationship between H_2O_2 concentration and the current; (c) A successive amperometric curve with different H_2O_2 concentrations (1, 10, 100 and 1000 μM) added into PBS successively at +0.3 V; (d) Corresponding linear relationship between the H_2O_2 concentration and current.

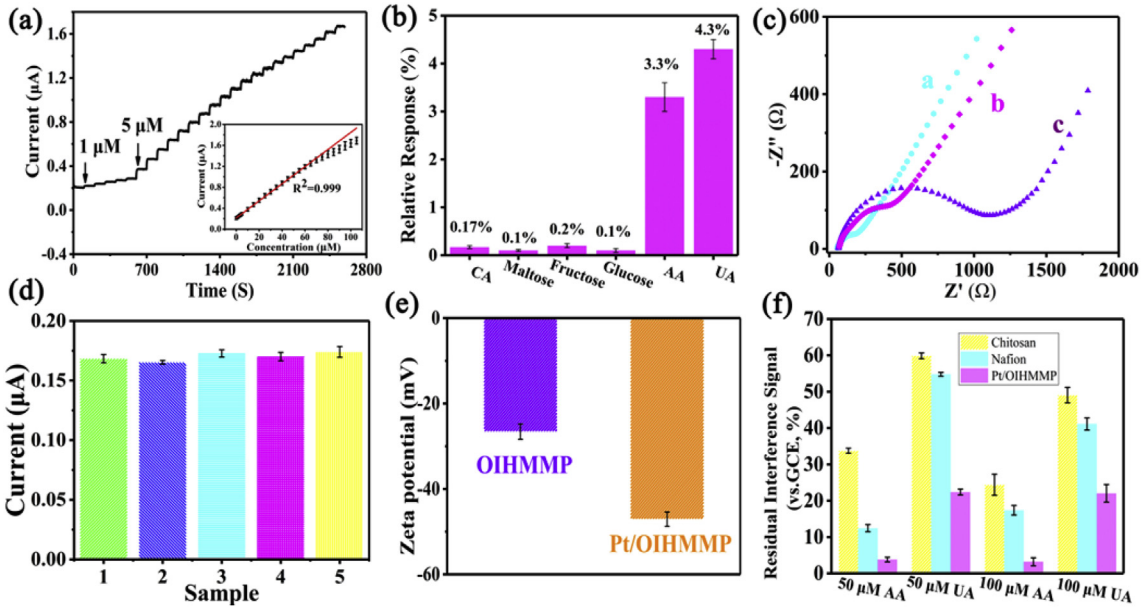

Fig. 4. (a) Amperometric curve with different sarcosine concentrations successively added into PBS at + 0.3 V. The inset shows the corresponding linear relationship between sarcosine concentration and current; (b) Interference columnar analysis of adding sarcosine (10 μM), maltose (100 μM), CA (100 μM), glucose (100 μM), AA (100 μM), fructose (100 μM) and UA (500 μM) successively in PBS at +0.3 V; (c) EIS responses in 0.1 M KCl containing potassium ferricyanide solution (5 mM): a. Pt/OIHMMP/GCE, b. bare GCE, c. SOx/Pt/OIHMMP/GCE; (d) Reproducibility of SOx/Pt/OIHMMP/GCE with 10 μM sarcosine; (e) Zeta potential of OIHMMP and Pt/OIHMMP; (f) The residual response signal of AA and UA on Chitosan/GCE, Nafion/GCE and Pt/OIHMMP/GCE compared with bare GCE.

excellent anti-interference ability. In addition, a standard titration method for exploring the application of this material in physiological environments is shown in Fig. S5 and Table S2 (using relationships depicted in the inset of Fig. 3d), indicating it is satisfactory in biological samples (Ju and Chen, 2015).

3.3. The electrochemical performance of SOx/Pt/OIHMMP/GCE for sarcosine

As described in section 3.2, Pt/OIHMMP displays excellent electrochemical performance for H_2O_2, which was crucial for the preparation of oxidase based biosensor. Next, a successive amperometric curve (Fig. 4a) indicated that SOx/Pt/OIHMMP/GCE has an outstanding response to sarcosine. Furthermore, the corresponding linear relationship between the response current and the concentration of sarcosine (the inset of Fig. 4a) has a linear range from 1 to 70 μM, and the linear regression equation is I(μA) = 0.01635 C(μM) + 0.21281 (R^2 = 0.999). The sensitivity and LOD are estimated to be 16.35 μA mM^{-1} (231.5 μA mM^{-1} cm^{-2}) and 0.13 μM (S/N = 3), respectively. Compared with some typical amperometric sarcosine biosensors (Table 1), the Pt/OIHMMP-based sarcosine biosensor is much better. Interference columnar analysis (Fig. 4b) indicates that there is almost no interference of maltose, glucose, CA and fructose. When AA(100 μM) and UA(500 μM) were injected, the interference signal changed 3.3% and 4.3% respectively, which showed practically little impact on this biosensor. Therefore, SOx/Pt/OIHMMP/GCE with good anti-interference ability is suitable for the application of sarcosine detection.

The electrochemical impedance spectroscopy (EIS), as an effective technique, was used to reflect the fabricated procedures of biosensor. As depicted in Fig. 4c, the electron-transfer resistance value was decreased with the successful combination of Pt/OIHMMP on the surface of bare GCE, manifesting that the electron transfer capacity was effectively enhanced by Pt/OIHMMP. In addition, the almost straight (curve a) indicate the electron transfer kinetics process of Pt/OIHMMP/GCE is diffusion-controlled (Chen et al., 2019), which was consistent with the result of Fig. 3a. After successfully combining SOx on the surface of Pt/OIHMMP/GCE, the electron-transfer resistance value was significantly increased, verifying it was effective immobilization as expected.

3.4. Analysis of real serum sample, reproducibility of SOx/Pt/OIHMMP/GCE

A standard titration method was performed to verify the physiological application of SOx/Pt/OIHMMP/GCE (Each sample was carried out for 5 times) in human serum. Standard concentration (10 μM, 20 μM, 30 μM) of sarcosine was added into the serum samples, as shown in Table S3. Using the linear relationship of Fig. 4a, the concentration of sarcosine in human serum was calculated. The recovery rate was 97.2–99.9%, revealing the accuracy of this method and the Pt/OIHMMP-based biosensor has potential application in detection of sarcosine in biological samples. To measure the reproducibility of SOx/Pt/OIHMMP/GCE, five sarcosine biosensors were fabricated

Table 1
Related parameters of typical amperometric sarcosine biosensors.

Materials	LOD (μM)	Linear range (μM)	Applied potential	Ref.
SOx/polyaniline film	Not mention	100–1000	0.4	Yang and Mu (1996)
SOx/PVA-Au-pphTEOS	500	500–7500	0.55	Lad et al. (2014)
SOx/Pt@ZIF8	1.06	5–30	0.4	Yang et al. (2018)
SOx/carbon screen printed electrodes	0.016	0.01–0.1	0.6	Rebelo et al. (2014)
SOx/Pt/MNP/GCE	0.24	5–40	0.4	Wang et al. (2019)
SOxNPs/AuE	0.01	0.1–100	1.0	Kumar et al. (2018)
SOx/Pt/OIHMMP/GCE	0.13	1–70	0.3	This work

individually for detection of 10 μM sarcosine under the uniform conditions (Fig. 4d), indicating anticipant reproducibility of the sarcosine biosensor.

3.5. Anti-interference performance test of SOx/Pt/OIHMMP/GCE

We anticipate that the surface potential of Pt/OIHMMP plays an important role in excluding anionic interferences. Zeta potential measurements (Fig. 4e) indicate that the surface potential of OIHMMP is −26.6 mV, which may be attributed to the electronegative phosphonic oxygen groups. For Pt/OIHMMP, the surface potential was found to be −47.1 mV due to the negative Pt particles (Chang et al., 2016). In addition, the zeta potential's results of interfering substances are showed in Fig. S6. Most interfering substances exhibit electronegativity in aqueous solution, and only aqueous solutions of sarcosine exhibit electropositive properties. Due to the substrate specificity of sarcosine oxidase, the biosensor exhibits good selectivity on distinguish of sarcosine from other interfering substances (Kumar et al., 2017, 2018). The contrast experiments regarding the anti-interfering performance of GCE, Nafion/GCE, Chitosan/GCE and Pt/OIHMMP/GCE are shown in Fig. 4f, using the current signal of the bare glass carbon electrode as the reference standard. Nafion, the most commonly used anti-interfering film, reduced the signal of AA (100 μM) by 82.64% (the residual signal is thus 17.36%) and the signal of UA (100 μM) by 58.90%, while the Pt/OIHMMP reduced their signals by 96.79% and 77.94%, respectively. The anti-interference ability of chitosan film is the worst. Only 75.62% and 50.94% of the interference signals can be reduced under the same conditions, respectively. That is, the residual signal from AA, compared with bare GCE, was 17.36% and 24.38% by using Nafion and chitosan, respectively, while it was only 3.21% by using Pt/OIHMMP, which clearly demonstrates the outstanding anti-interference ability of Pt/OIHMMP.

4. Conclusions

In conclusion, we describe a simple strategy for fabricating amperometric enzyme biosensors with strong anti-interference capabilities. Sarcosine oxidase was used as a model enzyme to prepare a sensitive (16.35 μA mM^{-1}, 231.5 μA mM^{-1} cm^{-2}), low LOD (0.13 μM) and wide linear range (1–70 μM) Pt/OIHMMP-based sarcosine biosensor. We verify that the surface potential of the carrier nanomaterial plays an important role in excluding anionic interferences. Compared with bare GCE, the residual signal of AA was 24.38% by using chitosan, 17.36% by using Nafion, and only 3.21% by using Pt/OIHMMP. This clearly demonstrates the outstanding anti-interference ability of Pt/OIHMMP. The electronegative mesoporous material may provide a biocomposite platform for the development of simple amperometric biosensors for μM level of substances in serum or urine.

Declaration of interests

The authors declare no competing financial interest.

CRediT authorship contribution statement

Qia Wang: Investigation, Formal analysis, Writing - original draft, Writing - review & editing. **Yuting Zhao:** Methodology, Writing - original draft, Writing - review & editing. **Qingui Yang:** Conceptualization. **Dan Du:** Writing - original draft, Writing - review & editing. **Haipeng Yang:** Supervision, Writing - original draft, Writing - review & editing, Funding acquisition. **Yuehe Lin:** Methodology, Conceptualization, Writing - original draft, Writing - review & editing.

Acknowledgement

The authors greatly appreciate the financial support from the Shenzhen Science and Technology Innovation Commission (Grant No. JCYJ20180305124343508) and the Postgraduate Innovation Development Fund Project of Shenzhen University (PIDFP-ZR2019027).

Appendix A. Supplementary data

Supplementary data to this article can be found online at https://doi.org/10.1016/j.bios.2019.111431.

References

Bai, Z.H., Li, G.Y., Liang, J.T., Su, J., Zhang, Y., Chen, H.Z., Huang, Y., Sui, W.G., Zhao, Y.X., 2016. Biosens. Bioelectron. 82, 185–194.
Benzigar, M.R., Talapaneni, S.N., Joseph, S., Ramadass, K., Singh, G., Scaranto, J., Ravon, U., Al-Bahily, K., Vinu, A., 2018. Chem. Soc. Rev. 47 (8), 2680–2721.
Chang, H.H., Zhang, H.C., Lv, J., Zhang, B., Wei, W.L., Guo, J.G., 2016. Biosens. Bioelectron. 86, 156–163.
Chen, Y., Yuan, P.X., Wang, A.J., Luo, X., Xue, Y., Zhang, L., Feng, J.J., 2019. Biosens. Bioelectron. 126, 187–192.
Chung, D.Y., Jun, S.W., Yoon, G., Kwon, S.G., Shin, D.Y., Seo, P., Yoo, J.M., Shin, H., Chung, Y.H., Kim, H., Mun, B.S., Lee, K.S., Lee, N.S., Yoo, S.J., Lim, D.H., Kang, K., Sung, Y.E., Hyeon, T., 2015. J. Am. Chem. Soc. 137 (49), 15478–15485.
Cui, J.W., Adeloju, S.B., Wu, Y.C., 2014. Anal. Chim. Acta 809, 134–140.
Damber, J.E., Aus, G., 2008. Lancet 371 (9625), 1710–1721.
Guo, S.J., Wen, D., Zhai, Y.M., Dong, S.J., Wang, E.K., 2010. ACS Nano 4 (7), 3959–3968.
Hassanipour-Azgomi, S., Mohammadian-Hafshejani, A., Ghoncheh, M., Towhidi, F., Jamehshorani, S., Salehiniya, H., 2016. Prostate Int. 4 (3), 118–124.
Hoffmann, F., Cornelius, M., Morell, J., Froba, M., 2006. Angew. Chem. Int. Ed. 45 (20), 3216–3251.
Huang, X.Q., Zhao, Z.P., Cao, L., Chen, Y., Zhu, E.B., Lin, Z.Y., Li, M.F., Yan, A.M., Zettl, A., Wang, Y.M., Duan, X.F., Mueller, T., Huang, Y., 2015. Science 348 (6240), 1230–1234.
Jiang, Y.Q., Cheng, X.L., Wang, C.A., Ma, Y.F., 2010. Anal. Chem. 82 (21), 9022–9027.
Ju, J., Chen, W., 2015. Anal. Chem. 87 (3), 1903–1910.
Kalantar-zadeh, K., Ou, J.Z., Daeneke, T., Strano, M.S., Pumera, M., Gras, S.L., 2015. Adv. Funct. Mater. 25 (32), 5086–5099.
Kumar, P., Jaiwal, R., Pundir, C.S., 2017. Anal. Biochem. 537, 41–49.
Kumar, P., Narwal, V., Jaiwal, R., Pundir, C.S., 2018. Biosens. Bioelectron. 122, 140–146.
Lad, U., Kale, G.M., Bryaskova, R., 2014. J. Electrochem. Soc. 161 (5), B98–B101.
Li, Y.S., Shi, J.L., 2014. Adv. Mater. 26 (20), 3176–3205.
Lilja, H., Ulmert, D., Vickers, A.J., 2008. Nat. Rev. Canc. 8 (4), 268–278.
Logozzi, M., Angelini, D.F., Iessi, E., Mizzoni, D., Di Raimo, R., Federici, C., Lugini, L., Borsellino, G., Gentilucci, A., Pierella, F., Marzio, V., Sciarra, A., Battistini, L., Fais, S., 2017. Cancer Lett. 403, 318–329.
Meyer, T.E., Fox, S.D., Issaq, H.J., Xu, X., Chu, L.W., Veenstra, T.D., Hsing, A.W., 2011. Anal. Chem. 83 (14), 5735–5740.
Narayanan, R., El-Sayed, M.A., 2004. Nano Lett. 4 (7), 1343–1348.
Narwal, V., Kumar, P., Joon, P., Pundir, C.S., 2018. Enzym. Microb. Technol. 113, 44–51.
Penson, D.F., Litwin, M.S., Aaronson, N.K., 2003. J. Urol. 169 (5), 1653–1661.
Rebelo, T., Pereira, C.M., Sales, M.G.F., Noronha, J.P., Costa-Rodrigues, J., Silva, F., Fernandes, M.H., 2014. Anal. Chim. Acta 850, 26–32.
Serra-Maia, R., Bellier, M., Chastka, S., Tranhuu, K., Subowo, A., Rimstidt, J.D., Usov, P.M., Morris, A.J., Michel, F.M., 2018. ACS Appl. Mater. Interfaces 10 (25), 21224–21234.
Shi, Q.R., Song, Y., Zhu, C.Z., Yang, H.P., Du, D., Lin, Y.H., 2015. ACS Appl. Mater. Interfaces 7 (43), 24288–24295.
Sing, K.S.W., Everett, D.H., Haul, R.A.W., Moscou, L., Pierotti, R.A., Rouquerol, J., Siemieniewska, T., 1985. Pure Appl. Chem. 57 (4), 603–619.
Song, Y.F., Hu, Q.H., Li, T.M., Sun, Y.K., Chen, X.X., Fan, J., 2018. Chem. Eng. J. 352, 163–172.
Sreekumar, A., Poisson, L.M., Rajendiran, T.M., Khan, A.P., Cao, Q., Yu, J.D., Laxman, B., Mehra, R., Lonigro, R.J., Li, Y., Nyati, M.K., Ahsan, A., Kalyana-Sundaram, S., Han, B., Cao, X.H., Byun, J., Omenn, G.S., Ghosh, D., Pennathur, S., Alexander, D.C., Berger, A., Shuster, J.R., Wei, J.T., Varambally, S., Beecher, C., Chinnaiyan, A.M., 2009. Nature 457 (7231), 910–914.
Sun, D.D., Lee, Y.S., Malhotra, A., Kim, H.K., Matecic, M., Evans, C., Jensen, R.V., Moskaluk, C.A., Dutta, A., 2011. Cancer Res. 71 (4), 1313–1324.
Thompson, I.M., Pauler, D.K., Goodman, P.J., Tangen, C.M., Lucia, M.S., Parnes, H.L., Minasian, L.M., Ford, L.G., Lippman, S.M., Crawford, E.D., Crowley, J.J., Coltman, C.A., 2004. N. Engl. J. Med. 350 (22), 2239–2246.
Tombach, B., Schneider, J., Matzkies, F., Schaefer, R.M., Chemnitius, G.C., 2001. Clin. Chim. Acta 312 (1–2), 129–134.
Walcarius, A., 2013. Chem. Soc. Rev. 42 (9), 4098–4140.
Wang, J., Ma, Q.Q., Wang, Y.Q., Li, Z.H., Li, Z.H., Yuan, Q., 2018. Chem. Soc. Rev. 47 (23), 8766–8803.
Wang, Q., Yang, C., Yang, Q.G., Yu, S.H., Yang, H.P., 2019. Anal. Chim. Acta 1046, 93–98.
Wei, J., Sun, Z.K., Luo, W., Li, Y.H., Elzatahry, A.A., Al-Enizi, A.M., Deng, Y.H., Zhao, D.Y., 2017. J. Am. Chem. Soc. 139 (5), 1706–1713.
Yang, H.P., Gao, G.W., Teng, F., Liu, W.J., Chen, S.J., Ge, Z.C., 2014. J. Electrochem. Soc. 161 (10), B216–B219.
Yang, H.P., Wang, J.J., Yang, C., Zhao, X.L., Xie, S.H., Ge, Z.C., 2018. J. Electrochem. Soc. 165 (5), H247–H250.
Yang, Y.F., Mu, S.L., 1996. J. Electroanal. Chem. 415 (1–2), 71–77.
Zhang, X.J., Ma, T.Y., Yuan, Z.Y., 2008. J. Mater. Chem. 18 (17), 2003–2010.
Zhou, Y.L., Yin, H.S., Meng, X.M., Xu, Z.N., Fu, Y.R., Ai, S.Y., 2012. Electrochim. Acta 71, 294–301.